**Paper No. PI:25**

**THE 13TH INTERNATIONAL STELLARATOR WORKSHOP**

# SHEAR ALFVÉN EIGENMODES IN COMPACT STELLARATORS

Spong[(1)], D.A., Sanchez[(2)], R., Weller[(3)], A., Hirshman[(1)], S.P.,
[1] *Oak Ridge National Laboratory, P.O. Box 2009, Oak Ridge, TN 37831-8073*
[2] *Universidad Carlos III de Madrid, Madrid, Spain*
[3] *Max-Planck-Institut für Plasmaphysik, IPP-Euratom, Garching, Germany*
*email: spongda@ornl.gov*

**Abstract.** The shear Alfvén continuum has been calculated for stellarators of arbitrary shape and aspect ratio using a symmetric matrix form of the continuum equation. Stellarators introduce strong poloidal/toroidal couplings in |B| and the $g^{\theta\theta}$ metric coefficient that can induce new continuum gap structures not present in axisymmetric tokamaks. Low field period period ($N_{fp}$ = 2 – 3), low aspect ratio devices result in strongly coupled toroidal mode families (n = $n_0$, $n_0 \pm N_{fp}$, $n_0 \pm 2N_{fp}$, etc.) that lead to HAE (Helical Alfvén Eigenmode) and MAE ( Mirror Alfvén Eigenmode) couplings at lower frequencies than are the case for larger aspect ratio, higher field period stellarator devices. Low field period configurations also have a higher density of coupled continua for a given frequency range; this characteristic could lead to higher levels of continuum damping.

## I. Introduction

Fast ion destabilized Alfvén modes[1] are of interest in stellarators since they can lead to enhanced fast ion losses and lowered heating efficiencies. In addition, these instabilities have potential diagnostic use (MHD spectroscopy), and may offer the possibility of directly channeling[2] fast ion energy to core ions through wave-particle mechanisms (i.e., bypassing the slower collisional transfer mechanisms). Low aspect ratio stellarators have stronger poloidal/toroidal/helical couplings in |B| and the $g^{\theta\theta}$ metric coefficient (which enter into the Alfvén continuum equation) than either tokamaks or large aspect ratio stellarators. Also, since low aspect ratio devices generally are designed at low field periods ($N_{fp}$ = 2 - 3), more closely spaced toroidal mode families must be taken into account in calculating the Alfvén spectrum. Although calculations have recently been presented of Alfvén continua in stellarators, these have generally been either only for large aspect ratio stellarators[3] or have assumed weak equilibrium couplings.[4] We have developed a calculation (the STELLGAP code) for analyzing the Alfvén continuum structure in compact devices and which can take into account interactions between multiple toroidal modes and retain an adequately resolved Fourier spectrum for the equilibrium quantities. This code uses Boozer coordinates and MPI parallelism over flux surfaces to allow both a high degree of radial and Fourier space resolution.

In the following, this calculation will be applied to both large and small aspect ratio stellarators. Calculation of the Alfvén continuum structure is the first step in predicting the frequency spectrum and stability properties of energetic particle destabilized modes in stellarators. Discrete roots with a global radial extent generally exist in the gaps between adjacent continuum frequencies; these discrete roots can be destabilized by energetic particles through inverse Landau damping when their velocity matches either the phase velocity of the stable discrete mode ($\sim v_A$) or its coupled sidebands. When such instabilities are near marginal stability, it is expected that if the mode's real frequency matches the frequency of

nearby continua, damping will result, increasing the threshold of the energetic particle pressure gradient required to drive these modes unstable. Studies of such effects in tokamaks[5] have shown good correlations between analytical continuum damping predictions [6] and non-perturbative numerical calculations[5] of Alfvén mode stability. Since stellarators offer a greater degree of design flexibility than tokamaks, it is expected that the calculation developed in this paper could ultimately be applied as an optimization target. Due to the fact that the Alfvén continuum structure is determined by the geometric and |B| couplings, it would be anticipated that these can be optimized in ways that could enhance continuum damping effects over at least limited ranges of frequency.

## II. Alfvén Continuum Equations and Solution Technique

The Alfvén continuum equation[7] in the incompressible limit (i.e., $\gamma = 0$, with no sound wave coupling) can be written as follows:

$$\omega_0 \omega^2 \frac{|\nabla\psi|^2}{B^2}\xi_s + \vec{B}\cdot\vec{\nabla}\left(\frac{|\nabla\psi|^2}{B^2}(\vec{B}\cdot\vec{\nabla})\xi_s\right) = 0 \tag{1}$$

where $\xi_s = \vec{\nabla}\cdot\left(\vec{B}\times\vec{\nabla}\psi\right)/\left|\vec{\nabla}\psi\right|^2$ = the surface displacement. We have solved the above equation in straight field line Boozer coordinates;[8] such coordinates preserve the zeros of the $\vec{B}\bullet\vec{\nabla}$ operator when coupled with a Fourier representation for $\xi_s$. The above equation can be expressed in these coordinates using the following relations:

$$\vec{B}\cdot\vec{\nabla} = \frac{1}{\sqrt{g}}\left(\iota\frac{\partial}{\partial\theta} + \frac{\partial}{\partial\zeta}\right) \quad \text{and} \quad \left|\vec{\nabla}\psi\right|^2 = g^{\psi\psi}\left(\frac{d\psi}{d\psi}\right)^2 \tag{2}$$

where $\theta$ is the poloidal coordinate, $\zeta$ is the toroidal coordinate, $\psi$ = the flux surface label, $g^{\psi\psi}$ = the contravariant $\psi\psi$ metric element and $\iota$ = the rotational transform. The eigenfunction $\xi_s$ can be expanded as:

$$\xi_s = \sum_{j=1}^{L}\xi_s^j e_j \quad \text{where} \quad e_j = \cos(n_j\zeta - m_j\theta) \tag{3}$$

For the calculation of Alfvén continua in devices with stellarator symmetry, one can consider the cos and sin components separately in the Fourier expansion of $\xi_s$ (due to the fact that they decouple). We have found that at least for cases we have checked, they both lead to the same set of contunua, so will only consider the only cos expansion of $\xi_s$ in this paper. Multiplying equation (1) by $\sqrt{g}e_i = \sqrt{g}\cos(n_i\zeta - m_i\theta)$ and doing a flux surface average, denoted by $\langle\cdots\rangle = \int_0^{2\pi}d\theta\int_0^{2\pi}d\zeta(\cdots)$ where $\sqrt{g}$ is the Jacobian, we obtain:

$$\omega_0\omega^2\left\langle e_i\sqrt{g}\frac{g^{\psi\psi}}{B^2}\sum_{j=1}^{L}\xi_j e_j\right\rangle + \left\langle e_i\left(\iota\frac{\partial}{\partial\theta} + \frac{\partial}{\partial\zeta}\right)\frac{g^{\psi\psi}}{B^2\sqrt{g}}\left(\iota\frac{\partial}{\partial\theta} + \frac{\partial}{\partial\zeta}\right)\sum_{j=1}^{L}\xi_j e_j\right\rangle = 0 \tag{4}$$

The second term in the above equation can then be integrated by parts to obtain the following matrix eigenvalue equation:

$$\lambda^2 \ddot{\mathbf{A}}\vec{\mathbf{x}} = \ddot{\mathbf{B}}\vec{\mathbf{x}}$$

$$\text{where} \quad \ddot{\mathbf{A}} = \left[a_{ij}\right] = \mu_0 \left\langle e_i \sqrt{g}\, \frac{g^{\psi\psi}}{B^2} e_j \right\rangle$$

$$\ddot{\mathbf{B}} = \left[b_{ij}\right] = \left\langle \frac{g^{\psi\psi}}{B^2\sqrt{g}} \left( \nabla_i \frac{\partial e_i}{\partial \psi} + \frac{\partial e_i}{\partial \theta} \nabla_i \frac{\partial e_j}{\partial \theta} + \frac{\partial e_j}{\partial \zeta} \right) \right\rangle \tag{5}$$

$$\vec{\mathbf{x}} = \left[\lambda_s^1 \;\; \lambda_s^2 \cdots \lambda_s^L\right]^T$$

The above matrix elements are obtained after expanding the following products of magnetic field components and metric elements in terms of Fourier series:

$$\frac{g^{\psi\psi}\sqrt{g}}{B^2} = \sum_{k=1}^{K} E_k \cos(n_k\theta - m_k\zeta), \qquad \frac{g^{\psi\psi}}{B^2\sqrt{g}} = \sum_{k=1}^{K} F_k \cos(n_k\theta - m_k\zeta) \tag{6}$$

The quantities on the left hand side of the above equations are initially calculated for each flux surface on a mesh in $\theta$ and $\zeta$ by forming the appropriate products and quotients of equilibrium quantities. This data is then transformed to the above Fourier space representations, keeping the shortest Fourier wavelength at least a factor of 2-3 larger than the mesh spacing to avoid anti–aliasing errors. The matrix elements then depend on two convolution integrals [other Fourier product combinations such as those involving $\cos(n_i\theta - m_i\zeta)\sin(n_j\theta - m_j\zeta)\cos(n_k\theta - m_k\zeta)$ and $\sin(n_i\theta - m_i\zeta)\sin(n_j\theta - m_j\zeta)\sin(n_k\theta - m_k\zeta)$ integrate to 0]:

$$I_{ccc}^{i,j,k} = \int_0^{2\pi} d\theta \int_0^{2\pi} d\zeta \cos\left(n_i\theta - m_i\zeta\right)\cos\left(n_j\theta - m_j\zeta\right)\cos\left(n_k\theta - m_k\zeta\right)$$

$$I_{ssc}^{i,j,k} = \int_0^{2\pi} d\theta \int_0^{2\pi} d\zeta \sin\left(n_i\theta - m_i\zeta\right)\sin\left(n_j\theta - m_j\zeta\right)\cos\left(n_k\theta - m_k\zeta\right) \tag{7}$$

Analytic algorithms have been developed (using the Mathematica[9] software) to provide these integrals for arbitrary combinations of the mode numbers $m_i$, $n_i$, $m_j$, $n_j$, $m_k$, $n_k$. These algorithms have been checked against independent calculations that use numerical integration. The advantage of the analytic algorithms is that they are exact and significantly faster. The required matrix elements may then be written as:

$$a_{ij} = \omega_0 \omega_{ion} \sum_{k=1}^{K} I_{ccc}^{i,j,k} E_k$$

$$b_{ij} = \sum_{k=1}^{K} I_{ssc}^{i,j,k} F_k \left[ \iota^2 m_i m_j + n_i n_j + \iota \left( m_i n_j + m_j n_i \right) \right] \tag{8}$$

Equation (1) has then been reduced to a symmetric matrix eigenvalue problem. We solve the above system of equations for all possible eigenvalues and eigenfunctions using the DSYGV routine from the IBM ESSL library.[10] It is expected that a higher performance continuum calculation (such as might be used within a stellarator optimization) can be obtained by calculating only a subset of the eigenvalues of the above equations (e.g., only for lower frequencies).

## III. Application of STELLGAP to High Aspect Ratio Stellarators

We have solved equation (1) for a variety of different stellarator configurations. In the absence of toroidal symmetry, the toroidal mode number is no longer a good quantum number and one must include a range of n's in the representation for the Alfvén eigenfunction, $\xi_s$. However, since this is a linear problem, the selection of n's is limited by the possible couplings from the dependence of the equilibrium to $n = n_0$, $n_0 \pm N_{fp}$, $n_0 \pm 2N_{fp}$, etc. where $n_0$ is the principal toroidal mode number of the set; in the following we refer this to as the $n = n_0$ mode family. For the examples given below, we typically include 20 poloidal modes and 10 toroidal modes in the representation of $\xi_s$. The equilibrium coefficients are also represented by 20 poloidal modes and 20 toroidal modes. For comparison purposes, we apply our code both to the full 3D stellarator configurations, retaining multiple n's in the representation of $\xi_s$ and to the same case with only the $n = n_0$ toroidal mode number present. The latter limit is effectively a tokamak limit in that only the n = 0 terms in the equilibrium will contribute to the matrix elements of equation (8).

We first apply the STELLGAP code to the W7-AS device.[11] The Alfvén continuum structure is calculated for discharge 42873; in this case Alfven activity was observed[11] for a frequency band of around 35 – 50 kHz. Transform and ion density profiles appropriate to this discharge have been used in the continuum calculation; the dominant ion species is deuterium. In Figure 1(a), the Alfvén gap structure is first displayed with only the n = 1 toroidal mode included. Color coding is used in Figures 1(a) and 1(b) to indicate which poloidal mode number is dominant in the eigenfunction for a given frequency and radial location. As may be seen, the plot with only n = 1 shows both low frequency toroidicity induced gaps (f = 20 – 50 kHz) as well as higher frequency gaps induced by non-circular shaping. In Fig. 1(b) we show the Alfvén gap structure including multiple n's in the representation for $\xi_s$. Here n = -19, -14, -9, -4, 1, 6, 11, 16, and 21 have been included, although the continua shown in Fig. 1(b) only involve n=1 and n = 6; the other n's enter in only at higher frequencies which are not plotted here. Next, in Fig. 2 the same continua as plotted in Figure 1(b) are displayed again, but with color coding used to indicate the dominant toroidal mode number. Here we have also indicated the frequency range for which Alfvén activity was observed in the experiment. All of the lower frequency gaps in this figure are TAE gaps; i.e., they involve only single toroidal mode number. At higher frequencies, helically induced gaps enter in and we have indicated the occurrence of one such gap at around $\omega/\omega_{max} = 0.4$ and 570 kHz.

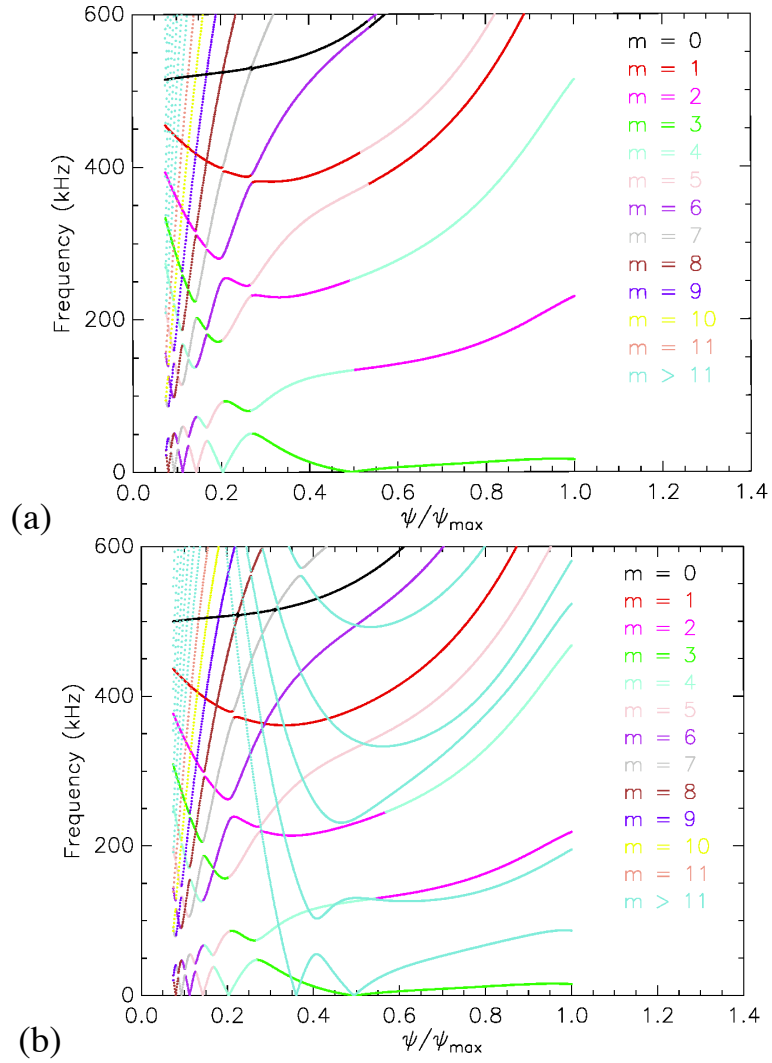


*Fig. 1 – Continuum gap structure for W7-AS case 42873 with color coding for the dominant poloidal mode number (a) using only n = 1, and (b) using the full stellarator equilibrium and toroidal mode numbers n = -19, -14, -9, -4, 1, 6, 11, 16, and 21.*

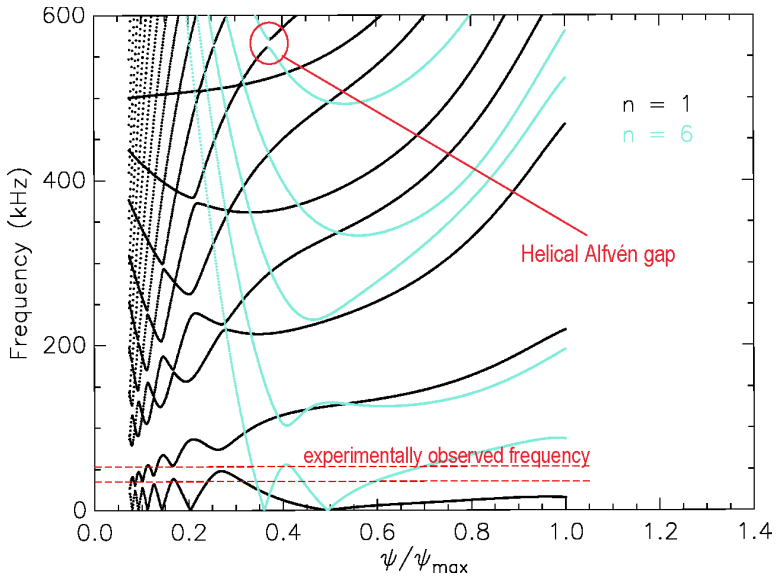

*Fig. 2 – Continuum gap structure for W7-AS case 42873 with color coding for the dominant toroidal mode number.*

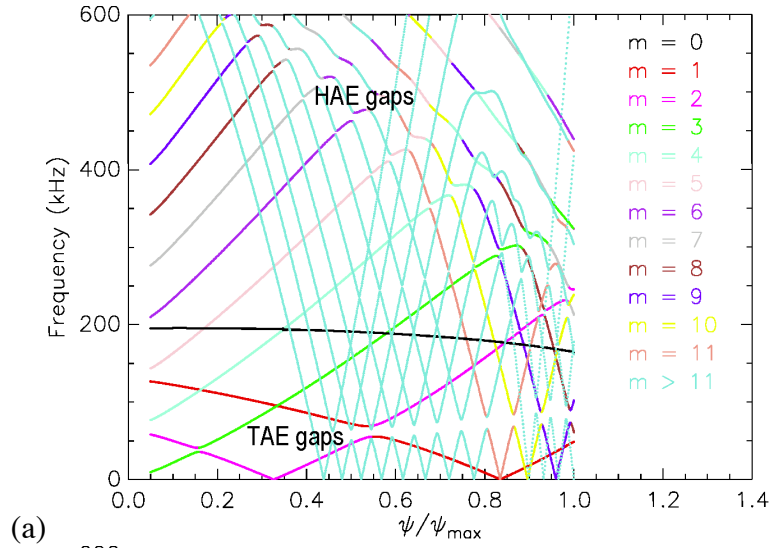


(a)

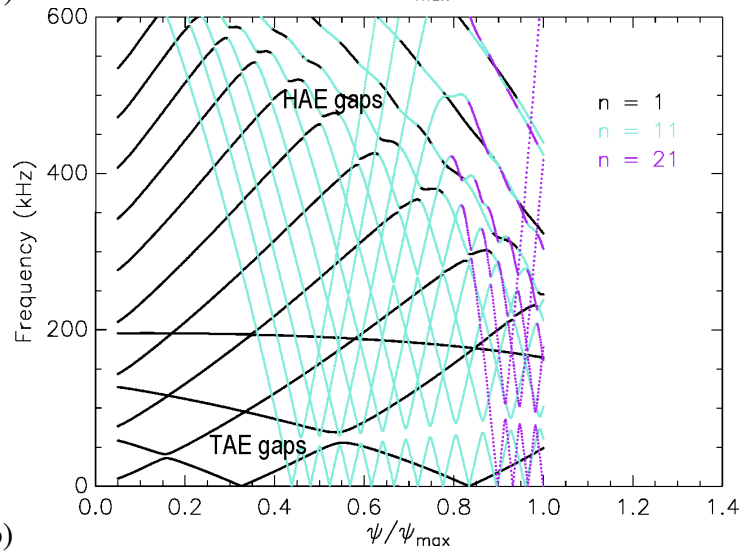


(b)

*Fig. 3 – Continuum gap structure for n = 1 mode family in LHD with color coding for the dominant poloidal mode number (a) with color coding for the dominant poloidal mode number, and (b) with color coding for the dominant toroidal mode number.*

In Figure 3 the continuum structure is calculated for the standard configuration of the LHD torsatron device.[12] Here a flat ion density profile has been assumed with the ion species taken as deuterium. Comparing Figure 3(a), which indicates the dominant poloidal mode numbers with Figure 3(b), which indicates the dominant toroidal mode numbers, it may be seen that the lower frequency gaps are again TAE gaps (induced by coupling of different m's at the same n) while the higher frequency gaps are HAE gaps (induced by coupling of different m's and n's).

## IV. Application of STELLGAP to Low Aspect Ratio Stellarators

Next, we calculate the continuum gap structure for two recent low aspect ratio stellarator designs. Compact stellarators can have substantially different Alfvén continuum structures than high aspect ratio stellarators for two reasons. First, the low aspect ratio results in much stronger couplings due to the significantly broader Fourier spectra of the equilibrium

quantities than is the case in the high aspect ratio configurations. Second, low aspect ratio devices generally are designed with fewer field periods than high aspect ratio devices. Since stellarator mode families are separated by $N_{fp}$, the number of field periods (i.e., $n = n_0$ $n_0 \pm N_{fp}$, $n_0 \pm 2N_{fp}$, etc.) low field period devices tend to have a higher density of continua for a fixed frequency range than higher aspect ratio devices.

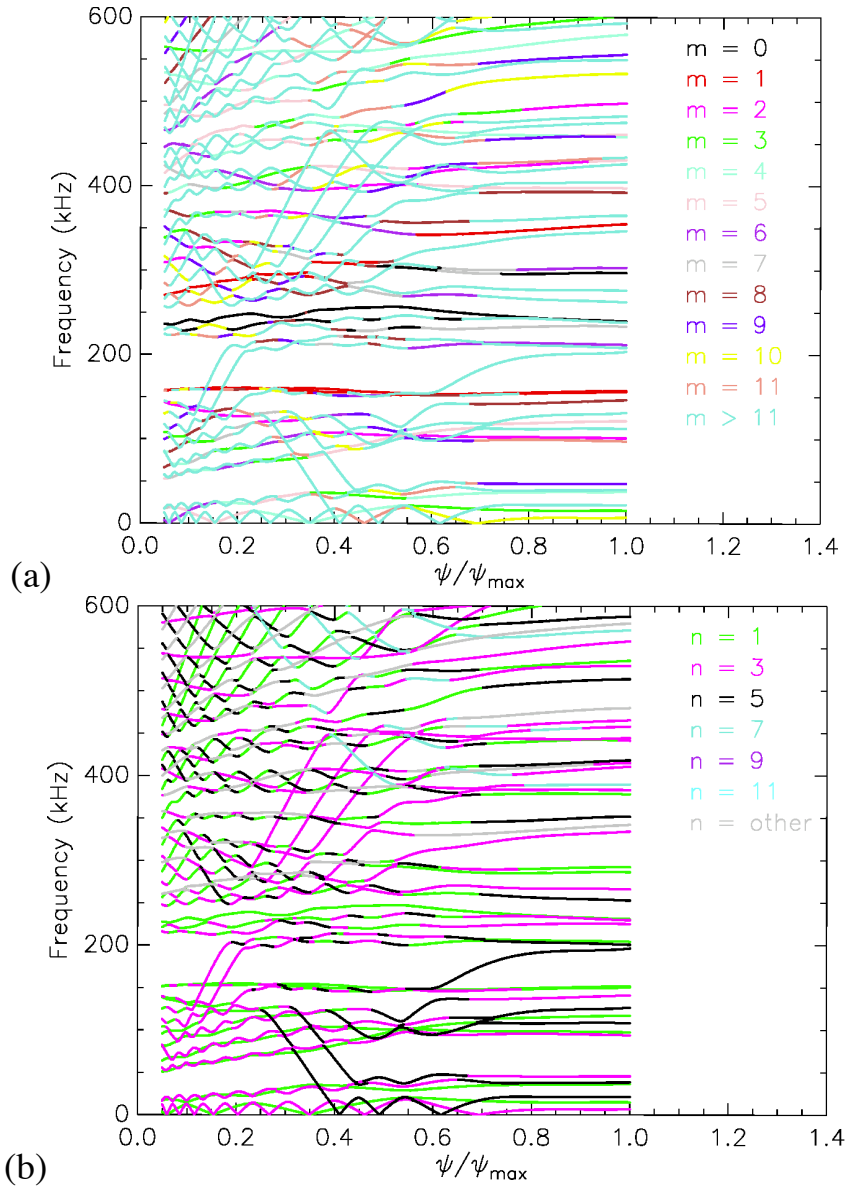


*Fig. 4 – Continuum gap structure for the QPS device (A = 2.7, $N_{fp}$ = 2) using the full stellarator equilibrium and toroidal mode numbers n = -11, …,1,…,13. Color coding is used to label (a) the dominant poloidal mode numbers, and (b) the dominant toroidal mode numbers.*

We first calculate continua for the QPS (Quasi Poloidal Stellarator) device.[13] This configuration has an aspect ratio of A = 2.7 and 2 field periods. The QPS has been optimized so that its |B| spectrum in Boozer coordinates is dominated by components with m□10,n□40. In Fig. 4 continua for the n = 1 mode family is plotted with the color coding used first to indicate the dominant poloidal mode number of the eigenfunction [Fig. 4(a)] and then the dominant toroidal mode number [Fig. 4(b)]. Again, we have used a flat ion density profile

with the ion species taken as deuterium. Except for a few of the lower continuum lines, most of the continuum gaps involve HAE couplings (i.e., modes with different m and n numbers are coupled). The presence of helically coupled gaps is evidenced by continua in Figure 4(b) that change color as one follows them outward in flux. Such gaps occur at lower frequencies and closer to the magnetic axis than for either of the large aspect ratio W7-AS or LHD devices.

Finally, in Figure 5 the continuum gap structure is calculated for the NCSX (National Compact Stellarator Experiment) device.[14] This configuration has an aspect ratio of A = 4.4 and 3 field periods. NCSX has been optimized so that its |B| spectrum in Boozer coordinates is dominated by components with m≠ 0,n=0 (i.e., the symmetry of a tokamak).

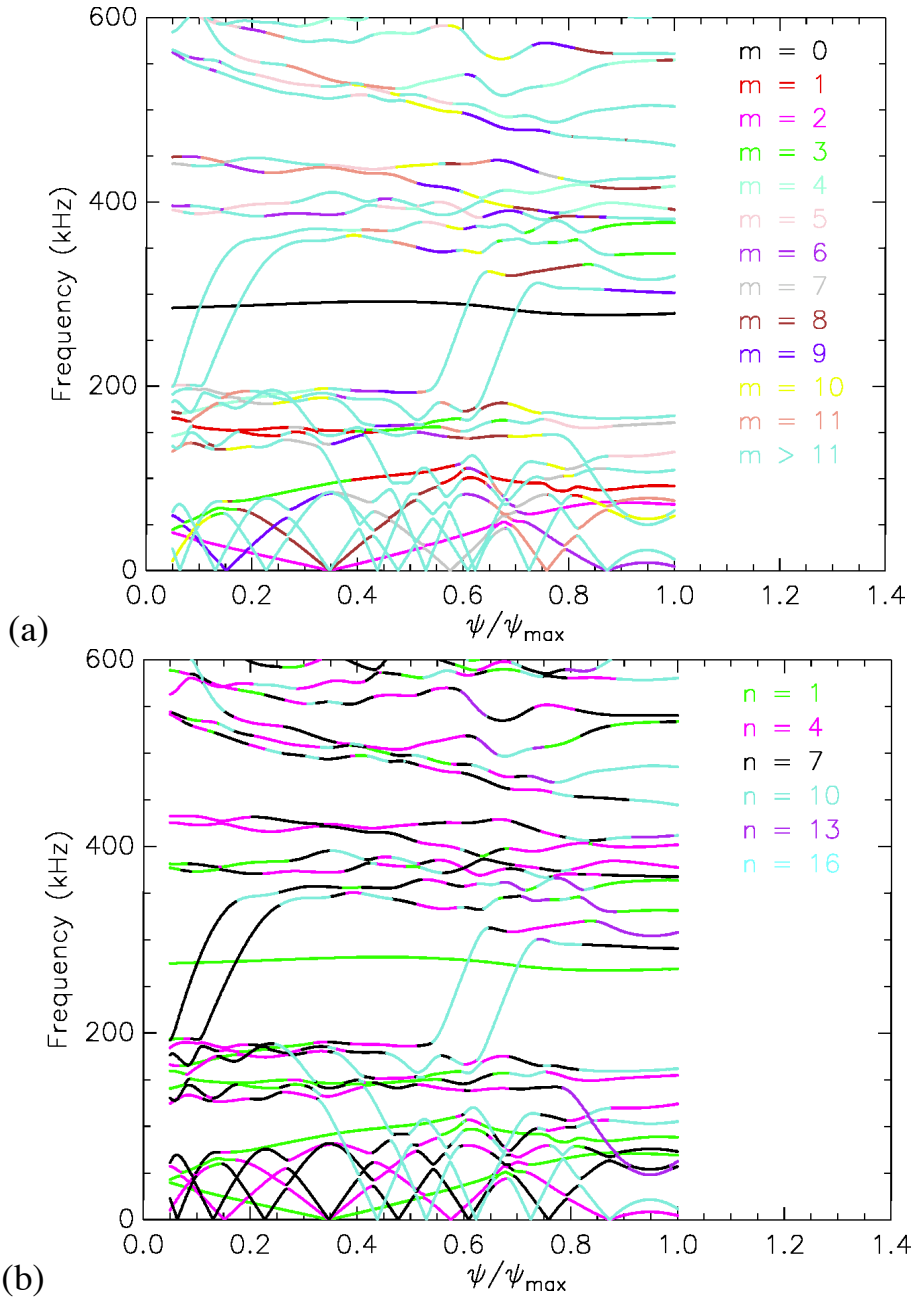


*Fig. 5 – Continuum gap structure for the NCSX device (A = 4.4, $N_{fp}$ = 3) using the full stellarator equilibrium and toroidal mode numbers n = -11, …,1,…,13. Color coding is used to label (a) the dominant poloidal mode numbers, and (b) the dominant toroidal mode numbers.*

A flat ion density profile has been used with the ion species taken as deuterium In Fig. 5 the continua for the n = 1 mode family are plotted with the color coding used first to indicate the dominant poloidal mode number of the eigenfunction [Fig. 5(a)] and then the dominant toroidal mode number [Fig. 5(b)]. Again, HAE-like couplings (different m and n) are clearly present except for some of the lower frequency continua. The density of continua is also high in comparison to the higher field period W7-AS and LHD devices, but not quite as high as the density of QPS continua in Figures 4(a) and (b).

## IV. Conclusions

A new method has been developed for calculating the 3D shear Alfvén continuum for stellarators of relatively arbitrary aspect ratio and shape. This calculation is carried out in Boozer coordinates[8] using equilibria generated by the VMEC[15] code. Calculation of the Alfvén continuum is the first step in addressing the stability of such modes in stellarators in the presence of fast ion components. In the future, we expect to extend the above methods to calculate the mode structure of the discrete roots lying in the continuum gaps and then examine their stability.

We find that the Alfvén continua in low aspect ratio, low field period devices are more complex than in higher aspect ratio configurations. Both TAE and HAE couplings are present and the density of continua over a given frequency range is higher due to the strong equilibrium couplings and the closer spacing ($\Delta n = N_{fp}$) between adjacently coupled toroidal modes in low field period devices. This characteristic may lead to stronger continuum damping of these modes in compact stellarators.

---

Acknowledgements: Work supported by U.S. Department of Energy under Contract DE-AC05-00OR22725 with UT-Battelle, LLC.

[1] C. Z. Cheng, M. S. Chance, Phys. Fluids **29**, 3695 (1986); G. Y. Fu, J. W. Van Dam, Phys. Fluids B **1**, 1949 (1989).
[2] N. J. Fisch, M. C. Herrmann, Nuclear Fusion **35**, 1753 (1995).
[3] C. Nührenberg, Phys. Plasmax **6**, 137 (1999).
[4] Ya. I. Kolsnichenko, V. V. Lutsenko, et al., Phys. Plasmas **8**, 491 (2001).
[5] D. A. Spong, B. A. Carreras, C. L. Hedrick, Phys. Fluids B **4**, 3316 (1992).
[6] M. N. Rosenbluth, H. L. Berk, et al., Phys. Rev. Lett. **68**, 596 (1992); F. Zonca, L. Chen, Phys. Rev. Lett. **68**, 592 (1992).
[7] A. Salat, J. A. Tataronis, Phys. Plasmas **8,** Part I 1200 (2001) and Part II 1207 (2001).
[8] A. H. Boozer, Phys. Fluids **24**, 1999 (1981).
[9] S. Wolfram, *The Mathematica Book*, Third Edition, Version 3, Cambridge Press (1996).
[10] Engineering and Scientific Subroutine Library for AIX Guide and Reference, 5765-C42, Document Number SA22-7272-03, Copyright IBM Corp., 1997 – 2000.
[11] A. Weller, et al., Phys. Plasmas **8**, 931 (2001).
[12] K. Toi, et al., Nuclear Fusion **40**, 1349 (2000).
[13] D. A. Spong, et al., Nuclear Fusion **41**, 711 (2001).
[14] A. Reiman, et al., Phys. of Plasmas **8**, 2083 (2001).
[15] S. P. Hirshman, J. C. Whitson, Phys. Fluids **26**, 3553 (1983).